energies

MDPI

Article

An Active Cascaded Battery Voltage Balancing Circuit Based on Multi-Winding Transformer with Small Magnetizing Inductance

Young-Hwa Park [1], Rae-Young Kim [2] and Yeong-Jun Choi [3,*]

[1] Hyundai & Kia Motors Namyang Institute, Hwaseong 18280, Korea; yhpark@hyundai.com
[2] The Department of Electrical and Biomedical Engineering, Hanyang University, Seoul 04763, Korea; rykim@hanyang.ac.kr
[3] The Department of Electrical Engineering, Jeju National University, Jeju 63243, Korea
* Correspondence: yeongjun.choi@jejunu.ac.kr; Tel.: +82-64-754-3677

Abstract: This paper covers the active voltage balancing method of secondary batteries. The number of applications using secondary batteries is increasing, and the batteries are normally connected in series/parallel to increase discharge cycle and power. The problem is that when there is a voltage imbalance between the cells or modules of a battery, there is a risk of an accident in the near-sighted way, shortening the life of the battery cells. Although this risk was prevented through passive balancing, this approach has limitations, including heat generation, long balancing time, and in the case of a battery that needs to be balanced between modules (or between stacks), its effectiveness decreases. Therefore, in this paper, an active cell balancing method that can overcome the limitations mentioned before is proposed. The proposed method uses a multi-winding transformer, and to increase the power density, the magnetizing inductance is decreased, and an auxiliary circuit is added. The validity of the proposed circuit was verified through mode analysis and simulation. In addition, waveforms showing the balancing performance under various conditions and the comparison results between conventional and proposed methods are given.

Keywords: active battery voltage balancing; battery management system; lithium-ion battery; multi-winding transformer

Citation: Park, Y.-H.; Kim, R.-Y.; Choi, Y.-J. An Active Cascaded Battery Voltage Balancing Circuit Based on Multi-Winding Transformer with Small Magnetizing Inductance. *Energies* **2021**, *14*, 1302. https://doi.org/10.3390/en14051302

Academic Editor: Carlos Miguel Costa

Received: 7 February 2021
Accepted: 22 February 2021
Published: 27 February 2021

1. Introduction

As interest in the environment increases and demand for eco-friendly energy increases, interest in energy storage devices is also increasing. Energy storage systems can be divided into mechanical energy-based and electro-chemical energy-based energy devices, according to the storage method and so on [1]. The method that is widely used in the industry is the electro-chemical energy-based energy storage system using a secondary battery [2]. Among many types of secondary batteries, lithium-ion batteries are especially widely used due to the advantages of high energy density and low self-discharge rate [2,3]. In general, secondary battery cells or modules (stacks) are connected in series or in parallel to increase the output power and discharge cycle of the energy storage device [4].

However, since the battery uses chemical energy, there are variations in charge/discharge characteristics, and due to this feature, each battery cell exhibits a voltage/SOC (state of charge) imbalance in repeated charge and discharge cycles [5]. The imbalance is a major factor deteriorating the performance and reliability of the energy storage system, and it may lead to an accident due to a reduction in battery capacity and overcharging. In order to prevent imbalance, an SOC-based balancing method based on the SOC estimation, as previously published in Ref. [6], and voltage-based balancing method can be adopted. Of the two methods, especially for lithium-ion batteries, a relatively simple voltage equalization circuit is being studied to overcome the voltage imbalance between battery cells.

Voltage equalization methods are classified into two categories: passive balancing methods and active balancing methods.

In the passive balancing method, a resistor and a switch are wired to each battery cell and the energy of the battery cell having a relatively high voltage is dissipated as heat. This method has disadvantages in terms of efficiency [7,8], and it also takes a long time to complete the balancing due to the current limitation of the voltage-sensing IC (integrated circuit).

To overcome this loss problem, an active balancing method can be considered. Unlike the passive balancing method, the active balancing method equalizes the voltage of the battery cells by transferring charges from the high-voltage battery cells to the low-voltage battery cells [9–27]. This method is divided into a charging shuttle method and a multi-winding transformer method. In the charge shuttle method, energy is stored in a capacitor or inductor through switching operations, which transfers the charge to the low-voltage cell [8–10]. This method involves a simple circuit configuration. However, since energy transfer is possible only between adjacent cells, it has the disadvantage that the balancing speed is slow.

As an alternative to this, the multi-winding transformer method sharing one magnetic core allows direct energy transfer between non-adjacent battery cells [12–19]. Studies in the literature [12–15] have proposed a method of selectively transferring the energy stored in the magnetizing inductor of a multi-winding transformer to a battery cell requiring charge equalization. In Ref. [16], a sensorless method was proposed in which all switches are turned on and off at the same time to achieve voltage balance. In addition, a method with an additional auxiliary circuit (for fast balancing) and a high-efficiency method with soft switching have been proposed [17,18]. The multi-winding transformer method requires a large magnetizing inductance to limit the balance current to the allowable charge/discharge current of the battery cell [20–24]. To obtain a large magnetizing inductance, it is necessary to increase the cross-sectional area of the core and the number of turns of the multi-winding transformer. This type of transformer has increased leakage inductance, which makes it difficult to design and maintain symmetry between windings. Moreover, it also increases prices and lowers power density.

In order to overcome this problem, in this paper, a multi-winding active voltage balancing circuit with a small magnetizing inductance that satisfies the allowable charge/discharge current value of a battery cell is proposed. The proposed circuit includes an additional diode and an inductor. When the main switch is turned on, the battery discharge current flows through the diode and the auxiliary inductor to reduce the size of the magnetizing inductor, and therefore power density is increased. By adopting this method, the allowable charging and discharging current values of the battery cells are limited by the auxiliary inductor. As such, the flexibility of the multi-winding transformer design is improved.

The reason why active cell balancing has not been widely applied despite various advantages and technological improvements is the increase in volume and cost. However, as the cost of cell replacement due to battery cell voltage imbalance continues to increase, the active balancing technique is becoming more significant. In particular, cell balancing needs to be re-considered. Therefore, this paper proposes a method with less power density reduction than the conventional method in order to lower the barriers against adopting battery cell balancing, and examines its feasibility. For the sequential explanation, this paper describes the balancing method that was previously proposed, analyzes the circuit and operation mode of the proposed method, and verifies its effectiveness through simulations based on the model derived from the frequency sweep results of battery.

2. Conventional Methods

2.1. Passive and Charge Shuttling Method

The battery voltage balancing method is classified into passive balancing and active balancing methods. In the passive balancing method, a resistor and a switch are wired to each battery cell and the energy of the battery cell with a relatively high voltage is dissipated as

heat. This method has a circuit configuration in which switches ($SW_1 \sim SW_4$) and resistors ($R_{bal1} \sim R_{bal4}$) are connected to each battery cell ($B_1 \sim B_4$), as shown in Figure 1.

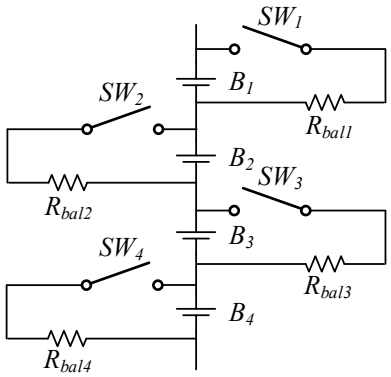

Figure 1. Passive balancing method.

This method works as follows. When charging battery modules connected in series, a battery with a high voltage may rise to a maximum allowable charging voltage, and a battery with a relatively low voltage may not increase to an allowable charging voltage. In order to fully charge the battery with a low voltage, the switch connected to the battery with a high voltage is turned on to dissipate energy through a series-connected resistor. That is, in order to equalize the voltage of all batteries, a switch connected to a battery cell with a relatively high voltage is turned on, and energy is dissipated as heat. Eventually, all batteries are charged up to the maximum allowable voltage. However, since excess energy is dissipated through the resistor, there is a disadvantage in that energy loss occurs, which can be as much as the voltage difference. In addition, there is the problem that loss increases when balancing between modules or stacks in this method. An active balancing method is a way to solve this limitation.

Unlike the passive balancing method, the active balancing method transfers energy from a high-voltage battery to a low-voltage battery with minimal energy loss. This method can be classified into charge shuttling and multi-winding transformer methods.

Figure 2 shows an inductive charge shuttling circuit. $SW_1 \sim SW_4$ represent switches, L_{bal1} and L_{bal2} represent balancing inductors and $B_1 \sim B_3$ represent battery cells [10]. In this method, energy is stored in an inductor through switching operations. The method has the advantage that it can be implemented with a simple circuit structure and a simple control operation, but has a disadvantage in that the balancing speed is slow because energy can be transferred only between adjacent battery cells. The method for overcoming this disadvantage is the multi-winding transformer method. The multi-winding transformer method directly transfers energy from a high-voltage battery to a low-voltage battery, so that voltage balancing is achieved at a faster rate compared to the charge shuttle method.

2.2. Multi-Winding Transformer Method

Figure 3 shows the voltage sensorless method, one of the multi-winding transformer methods. For the simple analysis, the battery is simplified into a model consisting of a voltage source ($e_{B1} \sim e_{Bn}$) and internal resistance ($R_{B1} \sim R_{Bn}$). In this method, the switches ($S_1 \sim S_n$) connected to each battery cell ($B_1 \sim B_n$) are turned on at a constant duty cycle, and a balancing operation is implemented by moving charges due to the voltage difference between cells, where L_{lkg} is the leakage inductance, V_p is the transformer tap voltage, L_m is the magnetizing inductance, i_{Reset} represents the reset current to prevent the saturation of the magnetizing inductance of the transformer, and D_{sn} and D are the body diodes of the switches and the diode on the secondary side of the transformer [16,17]. This method has the advantage that voltage sensing is not required, but it has the disadvantage that when the voltage difference decreases as the balancing operation proceeds, the balancing current decreases and the balancing speed becomes slow. As a method to overcome the

disadvantage of the balancing speed, there is the method of storing energy in a magnetizing inductor and selectively transferring energy to a battery cell with low voltage. Figure 4 shows one of these (the method of adding the auxiliary switch S_{n+1}) [12–15].

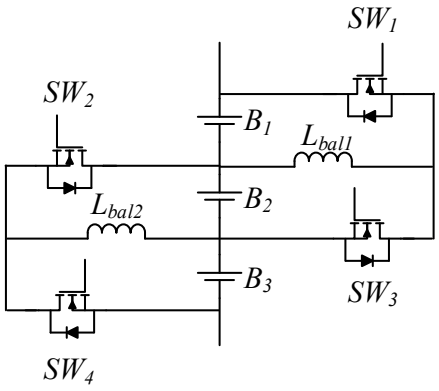

Figure 2. Inductive charge shuttling circuit.

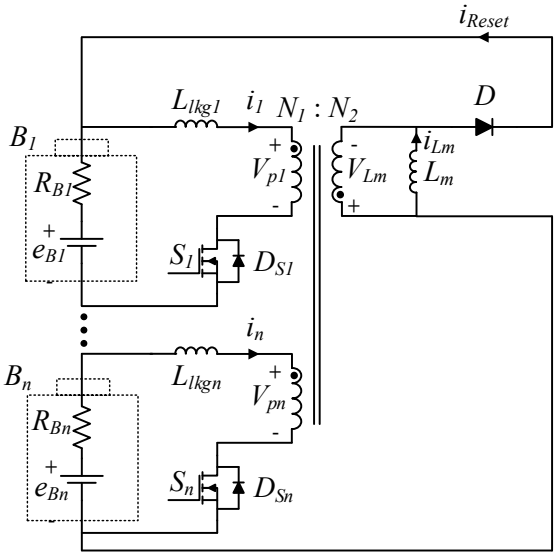

Figure 3. Voltage sensorless balancing method.

However, to adopt this method, it is necessary to increase the magnetizing inductance value to satisfy the allowable charge/discharge current value of the battery. As can be seen from Equation (1), since the magnetizing inductor is proportional to the number of turns N and the cross-sectional area A_c of the transformer core, it leads to an increase in the number of N and the use of a core with a wide A_c, where μ_0 denotes magnetic permeability of free space, μ_r denotes relative permeability and l denotes core length. If the number of windings increases, it is difficult to manage the leakage inductance and symmetry between windings, which increases the difficulty of transformer design. In addition, due to the large number of N and the wide A_c of the core, the volume of the transformer and of course the volume of the system are increased. In other words, it has the disadvantage of lowering the power density and increasing the cost.

$$L_m = \frac{\mu_0 \mu_r N^2 A_c}{l} \tag{1}$$

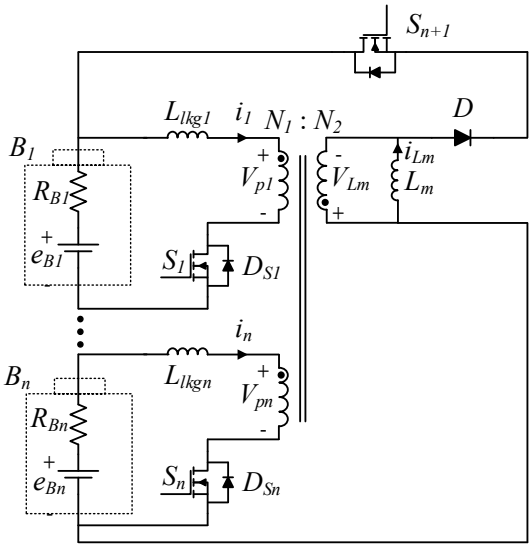

Figure 4. Voltage sensorless balancing method.

3. Proposed Method

3.1. Circuit Configuration and Operation Principle

In order to overcome the limitations of the aforementioned methods, in this paper, a novel multi-winding transformer voltage balancing circuit that prevents the excessive charge/discharge current of battery cells while using small magnetizing inductance by adding an auxiliary circuit is proposed. By adopting the proposed method, it is possible to increase the power density because an auxiliary inductor is used instead of a transformer's L_m. Actually, to design the transformer, it is necessary to consider multiple windings. When increasing the magnetizing inductance of the transformer, the cross-sectional area of the windings and the window area of the transformer core must be considered. Moreover, the size of the magnetic core does not increase in linear size. As such, the decrease in power density is further intensified as the magnetizing inductance increases. However, in the case of the auxiliary inductor, there is no related issue as regards the above problems.

Based on the cell selective voltage balancing method, the proposed circuit undergoes circuitry modification by adding an auxiliary circuit that includes a diode and an inductor. When the switch S_{main} is turned on, the discharge current of the battery connected in series flows to the auxiliary inductor instead of the magnetizing inductor of the multi-winding transformer. Therefore, the magnitude of the discharge current of the battery cell is determined by the auxiliary inductor, and the flexibility of the multi-winding transformer design is increased.

Figure 5 shows the proposed multi-winding transformer circuit based on a flyback DC–DC converter. Each of the open-circuit voltages $V_{B1} \sim V_{Bn}$ of the lithium-ion battery cells $B_1 \sim B_n$ is expressed by an electrical equivalent model, in which the voltage sources $e_{B1} \sim e_{Bn}$ and the internal resistors $R_{B1} \sim R_{Bn}$ are connected in series. V_{pack} represents the battery pack voltage. The charging and discharging currents of the battery cells are denoted as $i_{B1} \sim i_{Bn}$. The discharging and charging currents are denoted by i_{dis} and $i_1 \sim i_n$, respectively. In addition, i_{aux} represents the current flowing to the auxiliary inductor. The magnetizing inductance and the leakage inductance of the multi-winding transformer are represented by L_m and $L_{lkg1} \sim L_{lkgn}$, respectively, and the voltages are represented by V_{Lm} and $V_{lkg1} \sim V_{lkgn}$. The windings $N_1 \sim N_n$ are all the same, and the voltages applied to the windings are represented by $V_{p1} \sim V_{pn}$. These windings, located in the battery cells, are connected to cell switches $S_1 \sim S_n$ for selecting the low-voltage battery cells that require balancing. The winding N_{n+1}, located in the battery pack, is connected to an auxiliary circuit that consists of an inductor L_{aux}, which stores energy, and a diode D_{aux}, which limits the direction of the magnetizing inductor current i_{Lm}. The main switch S_{main} applies the

battery pack voltage V_{pack} to the auxiliary inductor L_{aux}; all switches have an anti-parallel diode D_n, and the forward voltage of the diode is indicated by V_{Dn}.

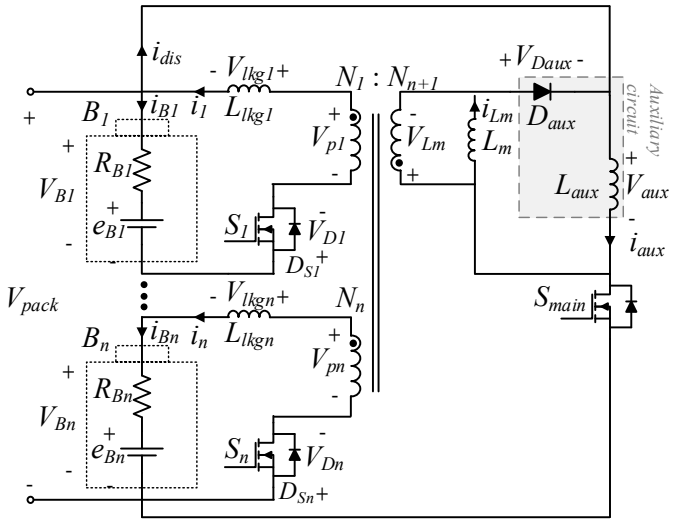

Figure 5. Proposed active voltage balancing circuit.

Figure 6 shows the flowchart depicting the operation of the proposed circuit. '*n*' denotes the number of battery cells connected in series; it is assumed that four battery cells are connected in series. V_{Band} denotes a predetermined voltage range, which is used to judge the completion of voltage equalization. When the voltage equalizing operation is started, all the switches are turned off and the open-circuit voltages $V_{B1} \sim V_{B4}$ are detected. When the voltage-detecting procedure is completed, the total average voltage $\overline{V_B}$ and the errors $V_{err1} \sim V_{err4}$ are calculated as expressed in (2) and (3), respectively.

If the error of the corresponding cell is greater than V_{Band}, the main switch and the cell switch of the corresponding cell are PWM (Pulse Width Modulation) - operated to perform the balancing operation. Alternatively, if the error is smaller than V_{Band}, the corresponding cell switch is turned off. Finally, when the errors $V_{err1} \sim V_{err4}$ are smaller than V_{Band}, achieved through the balancing operation of the circuit, the main switch S_{main} is turned off to complete the balancing operation.

$$\overline{V_B} = \frac{V_{B1} + V_{B2} + V_{B3} + V_{B4}}{4} \tag{2}$$

$$V_{err\_n} = \overline{V_B} - V_{Bn} \tag{3}$$

3.2. Mode Analysis

The PWM operation of the proposed circuit has four operation modes, as shown in Figure 7. In addition, several assumptions are given as follows to simplify the analysis:

- All leakage inductances of multi-winding transformers are equal to L_{lkg}, and have very small values;
- The internal resistance of all battery cells $R_{B1} \sim R_{B4}$ is negligibly small;
- The open-circuit voltages $V_{B1} \sim V_{Bn}$ and the average voltage are expressed as (4),

$$V_{B1} > V_{B2} > \overline{V_B} > V_{B3} > V_{B4} \tag{4}$$

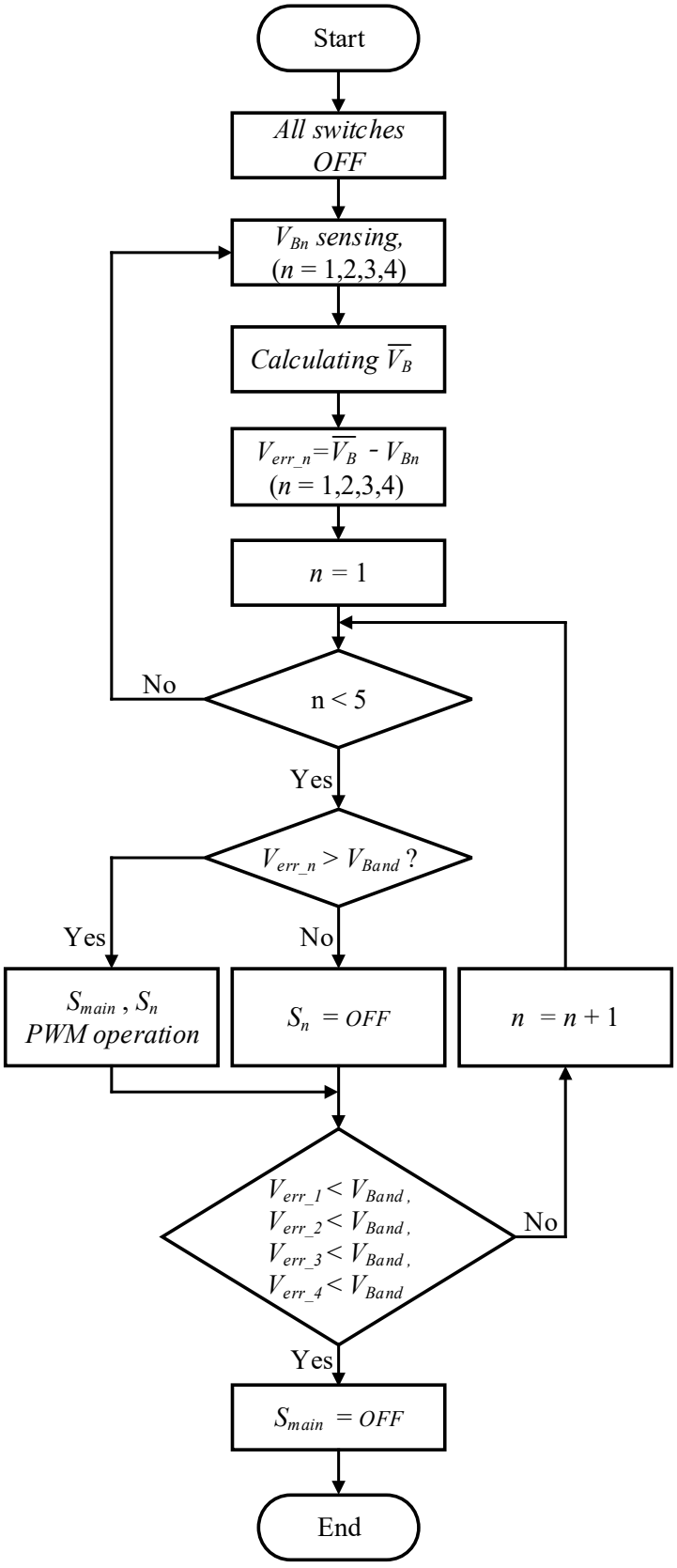

Figure 6. A flowchart for the proposed method.

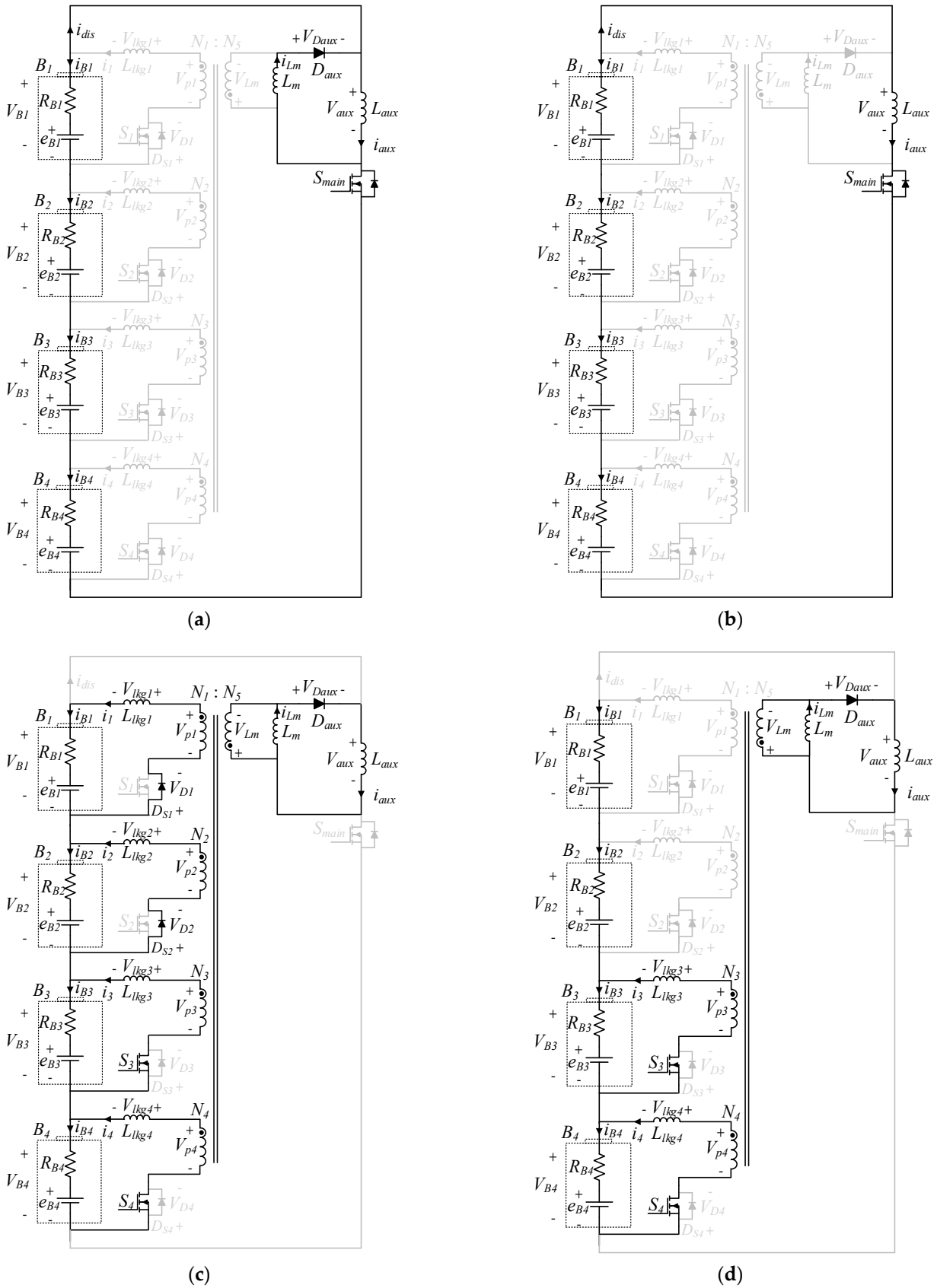

Figure 7. Operation modes of the proposed circuit: (**a**) mode 1, (**b**) mode 2, (**c**) mode 3, and (**d**) mode 4.

(1) Mode 1 (t_0 ~ t_1): Mode 1 starts with S_{main} turning on at t_0. When S_{main} is turned on, V_{pack} is applied to L_{aux}, and the auxiliary inductor current i_{aux} cannot flow to L_m by D_{aux}. At the same time, i_{aux} increases linearly, as shown in Figure 8a, and the slope is determined by L_{aux}. The discharge current i_{dis} of the battery pack is expressed as (5) through the voltage equations of L_{aux} and L_m. The i_{aux} from t_0 to t_1 is linearly increased and is expressed as (6).

$$\begin{aligned} i_{dis}(t) &= i_{aux}(t) - i_{Lm}(t) \\ &= \frac{V_{pack}}{L_{aux}}(t - t_0) + i_{dis}(t_0) - \left\{ \frac{V_{pack} + V_{Daux}}{L_m}(t - t_0) + i_{Lm}(t_0) \right\} \end{aligned} \tag{5}$$

$$i_{aux}(t) = \frac{V_{pack}}{L_{aux}}(t - t_0) + i_{dis}(t_0) \tag{6}$$

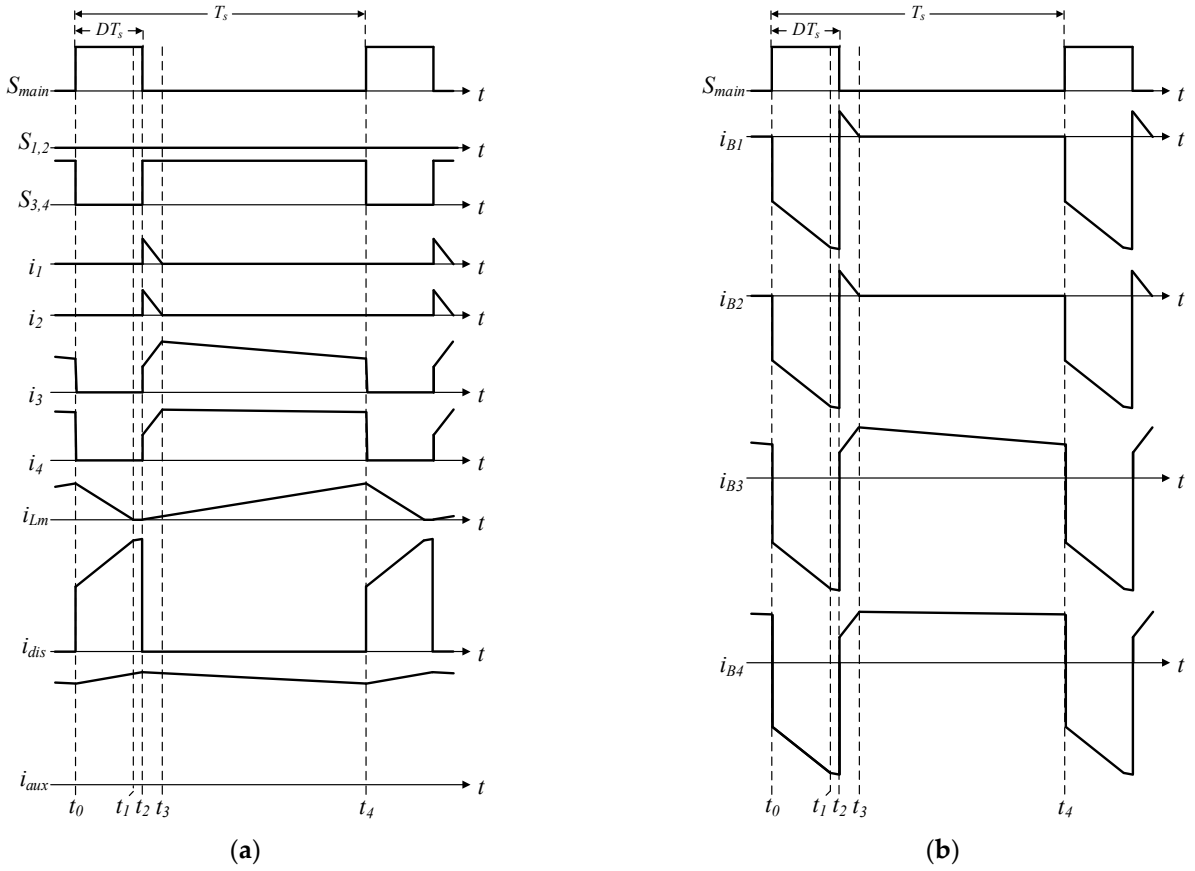

Figure 8. Key waveforms of the proposed circuit: (**a**) operating waveforms and (**b**) charge and discharge currents.

(2) Mode 2 (t_1 ~ t_2): Mode 2 begins at t_1 with i_{Lm}, and converges to zero. In this mode, D_{aux} is reverse-biased, and i_{dis} is equal to i_{aux}. The i_{dis} is expressed as (7), and the slope is determined by L_{aux}. The i_{aux} increases linearly in the same way as in Mode 1, as shown in (8); it has a maximum value of I_{max} at t_2, as shown in (9) and Figure 8a.

$$i_{dis}(t) = i_{aux}(t) = \frac{V_{pack}}{L_{aux}}(t - t_1) + i_{dis}(t_1) \tag{7}$$

$$i_{aux}(t) = \frac{V_{pack}}{L_{aux}}(t - t_1) + i_{dis}(t_1) \tag{8}$$

$$I_{\max}(t) = i_{aux}(t_2) \tag{9}$$

(3) Mode 3 ($t_2 \sim t_3$): Mode 3 starts at t_2, at which point S_{main} is turned off, and the lower-voltage battery side switches S_3 and S_4 (connected to B_3 and B_4) are simultaneously turned on. At t_3, the charging current of the battery cells is zero. As shown in Figure 8a, i_{aux} starts to decrease linearly at t_2. The equivalent circuit in Mode 3 is expressed as Figure 9a (since the transformer has the same winding ratio). As shown in the figure, i_{aux} is divided into a magnetizing inductor and battery cells $B_1 \sim B_4$ through a multi-winding transformer; thus, i_{aux} in Mode 3 is expressed as (10). In this case, $i_1 \sim i_4$ are expressed as (11) to (15). Since i_1 and i_2 flow through the anti-parallel diodes of the switch, the current value decreases, and i_3 and i_4 flow through the switch; this causes the current value to increase. In addition, $V_{lkg}1 \sim V_{lkg}4$ can be ignored because the leakage inductance of the transformer is assumed to be very small. In the case of Mode 3, the V_{aux}, which denotes the voltage across the auxiliary inductor, is V_{t3}, which is expressed as (15).

$$i_{aux}(t) = \frac{V_{t3}}{L_m}(t - t_2) + i_1(t) + i_2(t) + i_3(t) + i_4(t) \tag{10}$$

$$i_1(t) = \frac{V_{t3} - (V_{B1} + V_{D1})}{L_{lkg}}(t - t_2) + i_1(t_2) \tag{11}$$

$$i_2(t) = \frac{V_{t3} - (V_{B2} + V_{D2})}{L_{lkg}}(t - t_2) + i_2(t_2) \tag{12}$$

$$i_3(t) = \frac{V_{t3} - V_{B3}}{L_{lkg}}(t - t_2) + i_3(t_2) \tag{13}$$

$$i_4(t) = \frac{V_{t3} - V_{B4}}{L_{lkg}}(t - t_2) + i_4(t_2) \tag{14}$$

$$V_{t3} = \frac{V_{B1} + V_{B2} + V_{B3} + V_{B4} + V_{D1} + V_{D2}}{4} \tag{15}$$

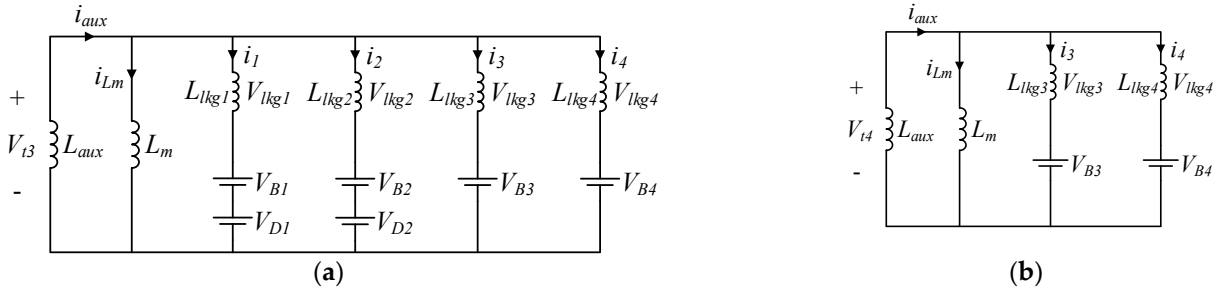

Figure 9. Equivalent circuits of the proposed circuit: (**a**) mode 3 and (**b**) mode 4.

Assuming that i_{Lm} is 0 at t_2 and that i_{aux} is evenly distributed to each battery cell (as shown in Figure 9a), $i_1 \sim i_4$ are expressed as (16).

$$i_1(t_2) = i_2(t_2) = i_3(t_2) = i_4(t_2) = \frac{I_{\max}}{4} \tag{16}$$

Δt_{M3} is defined as the difference between the points of t_2 and t_3, as shown in (17). Considering that V_{B1} is larger than V_{B2}, Δt_{M3} is expressed as (18).

$$\Delta t_{M3} = t_3 - t_2 \tag{17}$$

$$\Delta t_{M3} = -\frac{I_{\max}}{4}\frac{L_{lkg}}{V_{t3} - (V_{B1} + V_{D1})} \tag{18}$$

(4) Mode 4 ($t_3 \sim t_4$): Mode 4 starts from t_3 when both i_1 and i_2 are zero. Figure 7d shows the charge and discharge current waveforms of the battery cells $i_{B1} \sim i_{B4}$, and the

equivalent circuit is shown in Figure 9b. As shown in Figure 7d, the auxiliary inductor current i_{aux} no longer flows to i_1 and i_2; instead, it flows only to i_3, i_4, and i_{Lm}. In this mode, i_{aux} is expressed as (19), similarly to Mode 3.

$$i_{aux}(t) = \frac{V_{t4}}{L_m}(t - t_3) + i_{Lm}(t_3) + \frac{V_{t4} - V_{B3}}{L_{lkg}}(t - t_3) + i_3(t_3) + \frac{V_{t4} - V_{B4}}{L_{lkg}}(t - t_3) + i_4(t_3) \quad (19)$$

Since the initial values of i_{Lm}, i_3, and i_4 at t_3 are obtained using the value of Δt_{M3} obtained in Mode 3, they are expressed as (20), (21), and (22), respectively.

$$i_{Lm}(t_3) = \frac{V_{t3}}{L_m}\Delta t_{M3} \quad (20)$$

$$i_3(t_3) = \frac{V_{t3} - V_{B3}}{L_{lkg}}\Delta t_{M3} + \frac{I_{\max}}{4} \quad (21)$$

$$i_4(t_3) = \frac{V_{t3} - V_{B4}}{L_{lkg}}\Delta t_{M3} + \frac{I_{\max}}{4} \quad (22)$$

Since the S_3 and S_4 are turned on in Mode 4, V_{aux}, which denotes the voltage across the auxiliary inductor, is expressed as shown in (23) using V_{t4}. That is, if the number of turned-on switches is 'm' and the total sum of the battery cell voltages connected to the turned-on switches is V_{B_T}, the generalized V_{t4} is expressed as (24).

$$V_{t4} = \frac{V_{B3} + V_{B4}}{2} \quad (23)$$

$$V_{t4} = \frac{V_{B\_T}}{m} \quad (24)$$

When S_{main} is turned on at t_4, S_3 and S_4 are turned off at the same time, and the operation mode is switched to Mode 1. Eventually, V_{B1} and V_{B2} are decreased and V_{B3} and V_{B4} are increased through repeated mode operation, which leads to voltage equalization.

3.3. Selection of the Auxiliary Inductor of the Proposed Circuit

As shown in Figure 7, the auxiliary inductor current i_{aux} is the sum of i_{dis} and i_{Lm} in Mode 1. This is also equal to i_{dis} in Mode 2. Furthermore, i_{aux} is the sum of i_{Lm}, i_1, i_2, i_3, and i_4 in Mode 3, and i_{Lm}, i_3, and i_4 in Mode 4. Therefore, $\bar{i}_{aux}$,which is the average value of one cycle of i_{aux}, is always greater than or equal to the average charge and discharge currents $\bar{i}_{B1} \sim \bar{i}_{B4}$ of the battery cell; this feature is expressed in (25), where max () means the largest value among the internal variables.

$$\max\left(\bar{i}_{B1}, \bar{i}_{B2}, \bar{i}_{B3}, \bar{i}_{B4}\right) \le \bar{i}_{aux} \quad (25)$$

$\bar{i}_A$ is the allowable average charge and discharge currents of the battery, and the circuit is designed such that $\bar{i}_{aux}$ is smaller than $\bar{i}_A$ (as shown in (26)), and the average charge and discharge currents $\bar{i}_{B1} \sim \bar{i}_{B4}$ are smaller than the allowable average charge and discharge currents $\bar{i}_A$. This relationship is expressed as (27).

$$\bar{i}_{aux} \le \bar{i}_A \quad (26)$$

$$\max\left(\bar{i}_{B1}, \bar{i}_{B2}, \bar{i}_{B3}, \bar{i}_{B4}\right) \le \bar{i}_A \quad (27)$$

Since i_{aux} increases linearly in Modes 1 and 2 and decreases linearly in Modes 3 and 4, the average current $\bar{i}_{aux}$ flowing through the auxiliary inductor over one period is expressed as (28), where T_s is the switching period.

$$\bar{i}_{aux} = \frac{1}{T_s}\left[\begin{array}{l} \frac{i_{aux}(t_0)+i_{aux}(t_1)}{2}(t_1 - t_0) + \frac{i_{aux}(t_1)+i_{aux}(t_2)}{2}(t_2 - t_1) \\ + \frac{i_{aux}(t_2)+i_{aux}(t_3)}{2}(t_3 - t_2) + \frac{i_{aux}(t_3)+i_{aux}(t_4)}{2}(t_4 - t_3) \end{array}\right] \quad (28)$$

In each operation mode, the value of i_{aux} is derived as (29) based on (6), (8), (10), and (49), where D is the duty rate, and D' is 1-D.

$$\bar{i}_{aux} \approx \frac{V_{pack}}{2L_{aux}} D(3T_s + \Delta t_{M3}) + \frac{2}{L_m}\{V_{t4}(D'T_s - \Delta t_{M3}) + V_{t3}\Delta t_{M3}\} + \frac{V_{t3}}{2L_m} D'\Delta t_{M3} \quad (29)$$

Finally, by substituting (29) into (26), the auxiliary inductance value L_{aux}, which satisfies the allowable charge and discharge currents $\bar{i}_A$ of the battery, is obtained as (30), where 'A' is $A = \frac{2}{L_m}\{V_{t4}(D'T_s - \Delta t_{M3}) + V_{t3}\Delta t_{M3}\} + \frac{V_{t3}}{2L_m} D'\Delta t_{M3}$.

$$L_{aux} > \frac{V_{pack} D(3T_s + \Delta t_{M3})}{2(\bar{i}_A - A)} \quad (30)$$

4. Simulation Results

4.1. Simulation Configuration

To verify the performance of the proposed circuit for voltage-balancing operations and the charge and discharge current control of the battery, according to the presence or absence of the auxiliary circuit in various situations, simulations were performed with a battery pack consisting of four battery cells connected in series.

Table 1 shows the electrical parameters used in the simulation. The battery voltage was set according to the assumptions made in the mode analysis, and the first-order model based on the equivalent capacitor and equivalent series resistance is used. In order to use a value close to the actual equivalent capacitor and resistance during the simulation, the frequency sweep result of the battery pack that consists of 4 parallel and 10 series connections of the INR18650-29E cell, manufactured by SAMSUNG SDI, was adopted. This method and the results, including the approximated ones, are mentioned in Ref. [28] as shown in Figure 10, and have been modified to reflect the characteristics of a cell. In addition, in order to perform a faster simulation, the value was adjusted to 1/100.

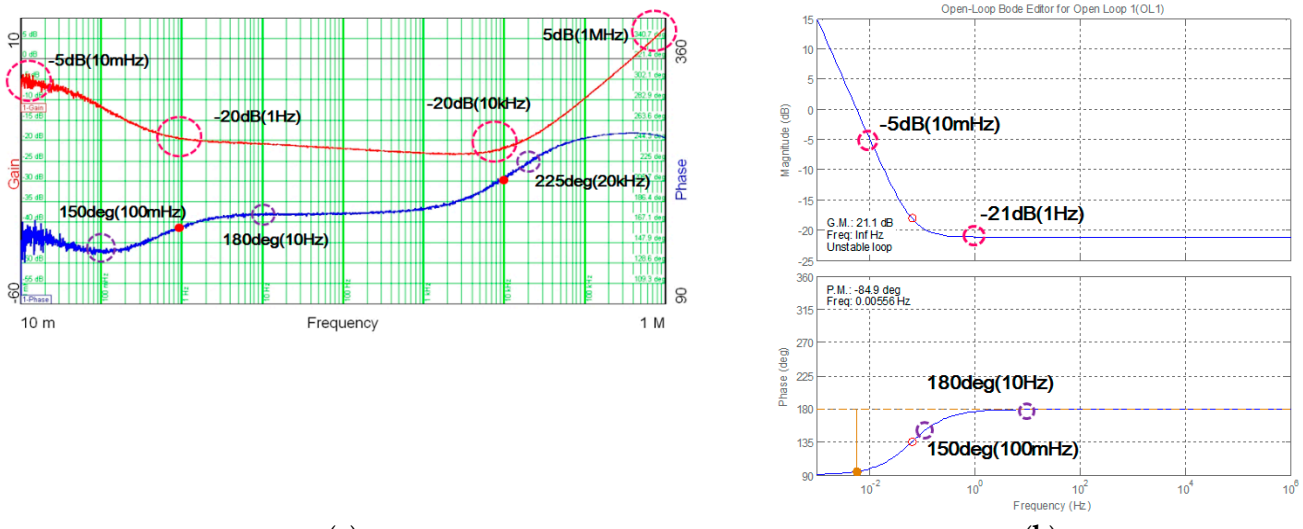

(**a**) (**b**)

Figure 10. Measurement and approximation results of the frequency response of the battery pack at the nominal voltage: (**a**) measurement and (**b**) approximation [28].

The allowable charge and discharge currents $\bar{i}_A$ are set to 2 A as an example. Thus, L_{aux} is selected to be larger than 0.13 mH by using (30). In this simulation, consequently, 1 mH was selected by considering a sufficient margin. Additionally, the values such as the magnetization inductance and leakage inductance, and the voltage drop values of the

antiparallel di and auxiliary diode, are measured or referred from the datasheet, and the value of V_{Band} is set to 1 mV.

Table 1. Simulation parameters.

Parameter	Value	Parameter	Value
V_{B1}	3.900 V	L_m	0.1 mH
V_{B2}	3.895 V	L_{aux}	1 mH
V_{B3}	3.750 V	$L_{lkg1} \sim L_{lkg4}$	0.59 µH
V_{B4}	3.700 V	$V_{D1} \sim V_{D4}$	0.8 V
$C_{B1} \sim C_{B4}$	718 mF	V_{Daux}	0.5 V
$R_{B1} \sim R_{B4}$	34.803 mΩ	-	-

4.2. Simulation Results and Review

Figure 11 shows the simulated operating waveforms of the proposed circuit. It can be seen from Figure 8a that the simulation results are the same as the theoretical waveforms.

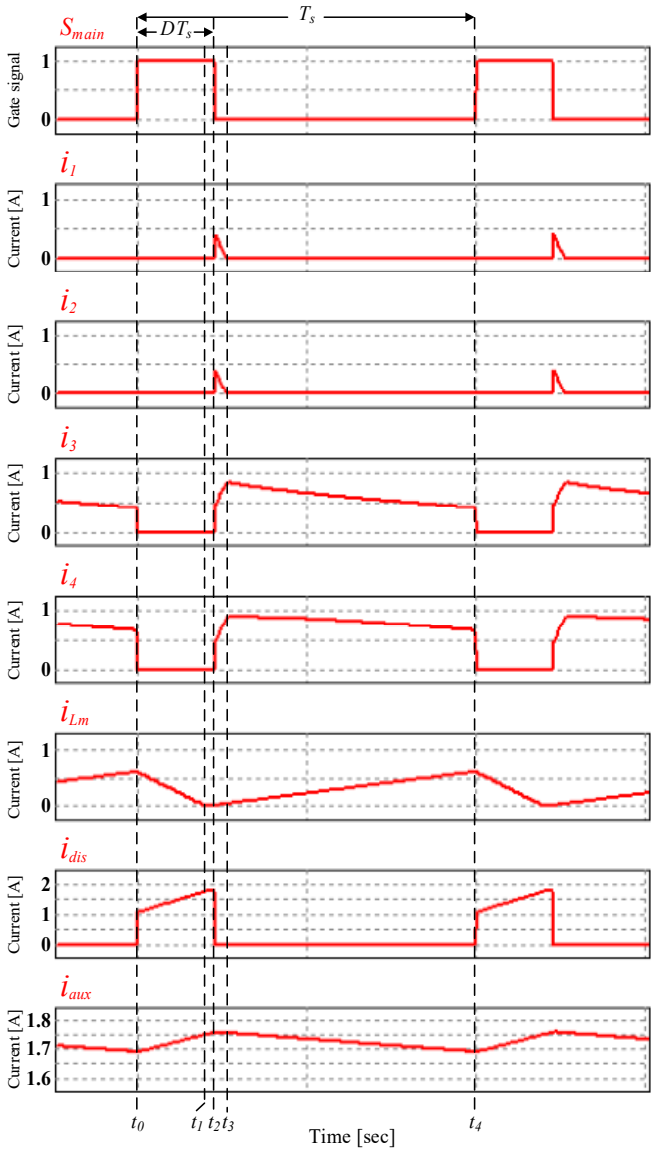

Figure 11. Simulated operating waveforms of the proposed circuit.

Figure 12a–c show the voltage balancing simulation results of the standalone operation, and the charging and discharging status of the proposed circuit. As can be seen from the simulation result, through the balancing operation, the energy of B_1 and B_2, which have relatively high voltages, was transferred to B_3 and B_4, that is, the voltage of the entire battery was converged. The gap that occurs after convergence is the V_{band} value. In summary, it is shown that adopting the proposed circuit enables voltage equalization under various operating conditions.

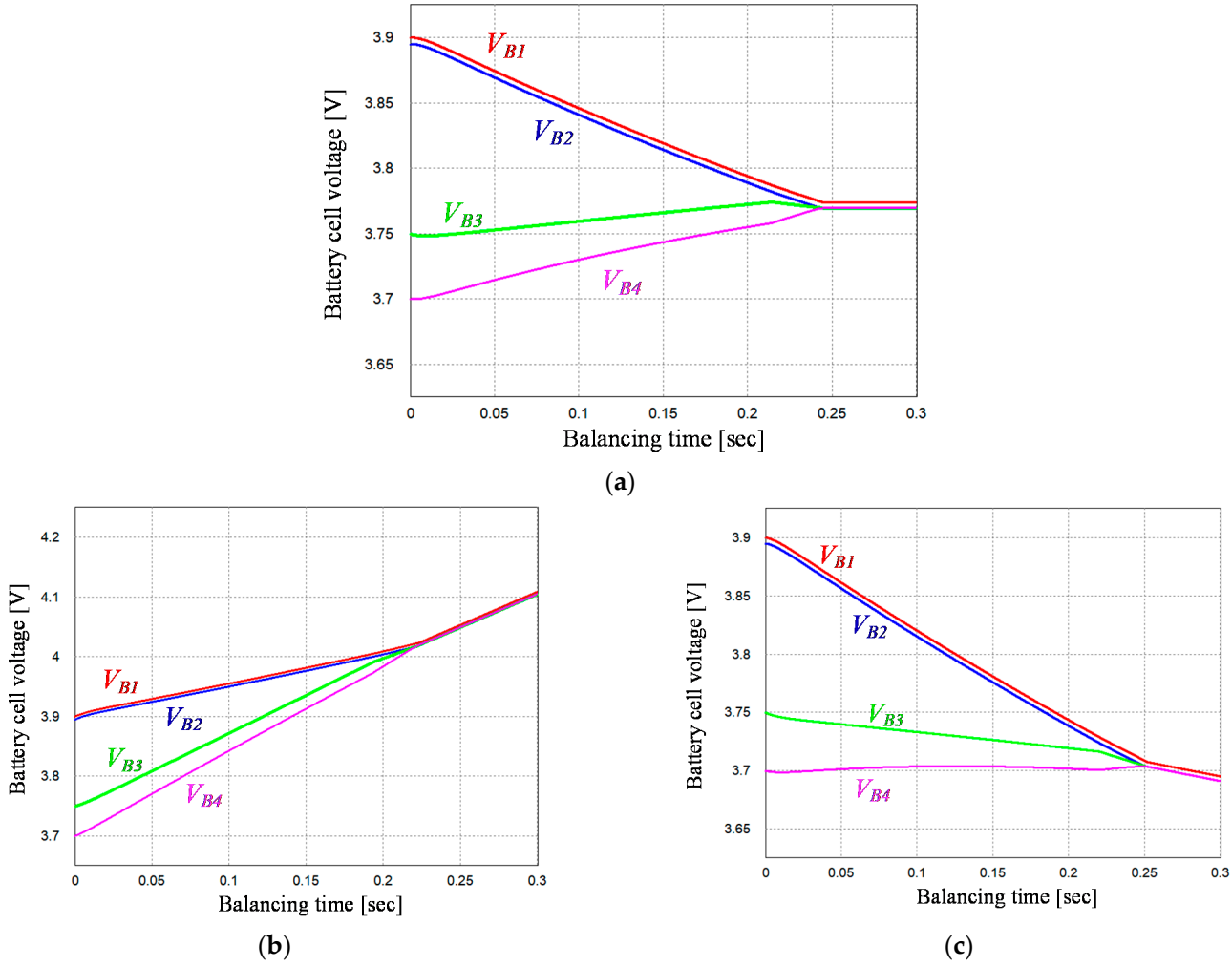

Figure 12. Simulation results of the proposed circuit in various conditions: (**a**) standalone condition, (**b**) charging condition, and (**c**) discharging condition.

Figures 13 and 14 show the charge and discharge currents with and without the auxiliary circuit of the proposed circuit. For adequate comparison, the magnetizing inductance L_m is set to 1.1mH for the case without the auxiliary circuit (to have the same inductance as the proposed circuit). The proposed circuit has a discharge current of 1.68 A and charge currents of 0.41 A, 0.41 A, 0.73 A, and 0.76 A for each battery cell, as shown in Figure 14. Without a proposed circuit, the discharge current is 3.45 A, and the charging currents are 0.85 A, 0.85 A, 1.59 A, and 1.67 A for each battery cell, as shown in Figure 14.

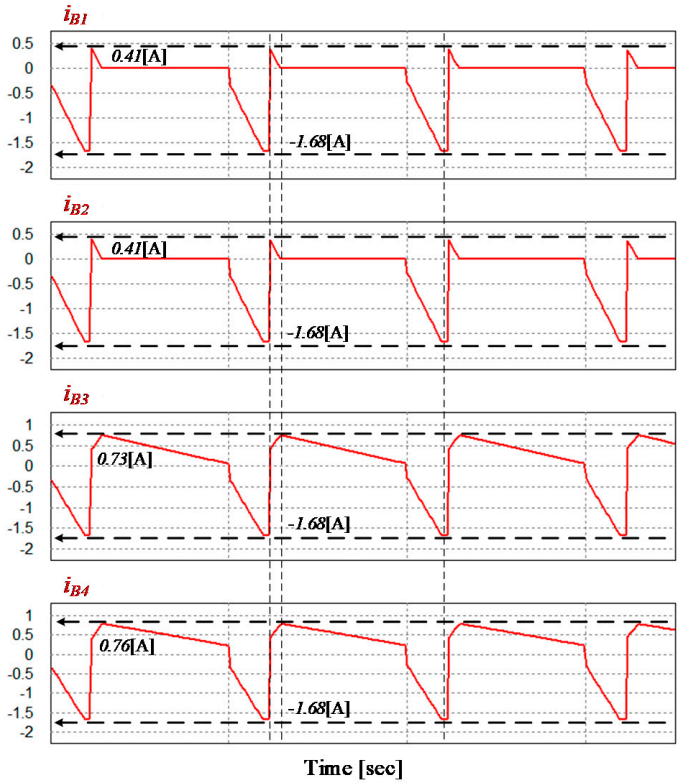

Figure 13. Simulation results of the proposed circuit (L_m: 0.1 mH, L_{aux}: 1 mH).

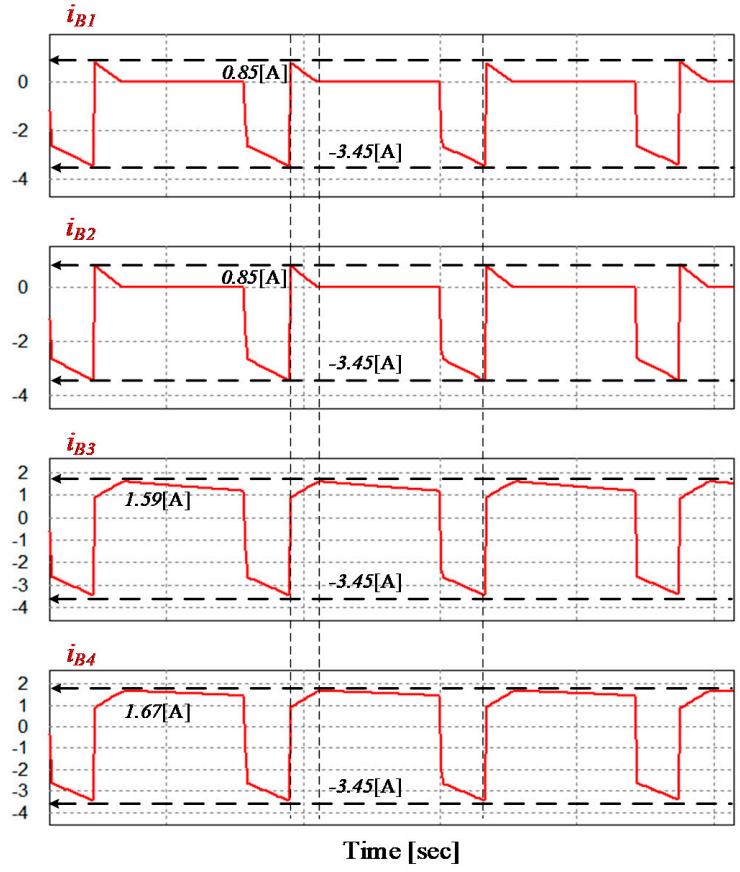

Figure 14. Simulation results without the auxiliary circuit (L_m: 1.1 mH).

The simulation results show that the current peaks with or without the proposed circuit are 1.68 A and 3.45 A (i.e., a reduction of 51.3% is observed). In terms of the charging current, when comparing the peak values of each battery cell's currents, the charging currents are reduced by about 52%, 52%, 54%, and 55%, respectively, when an auxiliary circuit is used.

In other words, the proposed circuit with the auxiliary circuit has lower charge and discharge currents than the circuit without the auxiliary circuit (under the same inductance condition); thus, the proposed circuit operates under a small magnetization inductance, which increases the design flexibility. In addition, the charge and discharge currents flowing into the battery are also within the set of allowable charge and discharge currents (i.e., 2 A), which means the value of the auxiliary inductance is properly designed.

5. Conclusions

This paper proposes an active battery voltage balancing method to overcome the voltage imbalance between cells or the modules of a battery that occurs when using secondary batteries. Although active voltage balancing has many advantages, it has not received attention so far due to its limitations in terms of cost and power density. However, with the expansion of applications for secondary batteries, securing safety and reliability is ultimately directly linked to other cost problems, and so the active balancing method is drawing attention again.

From this point of view, this paper proposes a multi-winding transformer-based battery voltage balancing circuit. The proposed circuit satisfies the allowable charge/discharge current of the battery cell even with a small magnetizing inductance through the voltage equalization operation using an auxiliary circuit. In addition, since the battery discharge current flows through the auxiliary inductor instead of the magnetizing inductor of the transformer, it operates with a small magnetizing inductance value, making it easy to manufacture the transformer, increasing the overall system power density and design flexibility.

The validity of the proposed circuit was verified through simulation. In the simulation, a comparative analysis of the conventional circuit, with a magnetizing inductance of 1.1 mH, and the proposed circuit with a magnetizing inductance of 0.1 mH and an auxiliary inductor of 1 mH was also performed. As a result of verification, the peak value of the discharge current decreased by about 51.3%, from 3.45 A to 1.68 A, and the peak value of the charging current decreased by 55% from 1.67 A to 0.76 A compared to the conventional circuit. In addition, the proposed method can be operated during charging/discharging, so it has an advantage in terms of utilization.

In addition, this method can be used for module/stack voltage balancing, and can be applied to various types of secondary batteries as well as lithium-ion batteries, so it will be used in various industrial fields.

Author Contributions: Conceptualization, Y.-H.P., R.-Y.K. and Y.-J.C.; methodology, Y.-H.P., Y.-J.C.; software, Y.-H.P. and R.-Y.K.; validation, Y.-H.P., R.-Y.K. and Y.-J.C.; formal analysis, Y.-H.P., R.-Y.K. and Y.-J.C.; investigation, Y.-H.P.; resources, R.-Y.K.; data curation, Y.-H.P., R.-Y.K.; writing—original draft preparation, Y.-H.P. and R.-Y.K.; writing—review and editing, Y.-H.P. and Y.-J.C.; visualization, Y.-H.P., R.-Y.K.; supervision, Y.-J.C.; project administration, R.-Y.K. and Y.-J.C. All authors have read and agreed to the published version of the manuscript.

Funding: This research received no external funding.

Institutional Review Board Statement: Not applicable.

Informed Consent Statement: Not applicable.

Data Availability Statement: Not applicable.

Conflicts of Interest: The authors declare no conflict of interest.

References

1. Hannan, M.A.; Hoque, M.M.; Mohamed, A.; Ayob, A. Review of energy storage systems for electric vehicle applications: Issues and challenges. *Renew. Sustain. Energy Rev.* **2017**, *69*, 771–789. [CrossRef]
2. Chris, M.; Masrur, M.A.; Gao, D.W. Batteries, Ultracapacitors, Fuel Cells, and Controls. In *Hybrid Electric Vehicles: Principles and Applications with Practical Perspectives*; Wiley: New York, NJ, USA, 2011; pp. 315–321. ISBN 978-0-470-74773-5.
3. Williamson, M. Air Power the Rise of Electric Aircraft. *Eng. Technol.* **2014**, *9*, 77–79. [CrossRef]
4. Emadi, A.; Joo Lee, Y.; Rajashekara, K. Power electronics and motor drives in electric, hybrid electric, and plug-in hybrid electric vehicles. *IEEE Trans. Ind. Electron.* **2008**, *55*, 2237–2245. [CrossRef]
5. Schuster, S.F.; Brand, M.J.; Berg, P.; Gleissenberger, M.; Jossena, A. Lithium-ion cell-to-cell variation during battery electric vehicle operation. *J. Power Sources* **2015**, *297*, 242–251. [CrossRef]
6. Wei, Z.; Dong, G.; Zhang, X.; Pou, J.; Quan, Z.; He, H. Noise-immune model identification and state of charge estimation for lithium-ion battery using bilinear parameterization. *IEEE Trans. Ind. Electron.* **2020**, *68*, 312–323. [CrossRef]
7. Kutkut, N.H.; Wiegman, H.L.N.; Divan, D.M.; Novotny, D.W. Charge equalization for an electric vehicle battery system. *IEEE Trans. Aerosp. Electron. Syst.* **1998**, *34*, 235–246. [CrossRef]
8. Weicker, P. *A Systems Approach to Lithium-Ion Battery Management*; Artech House: Norwood, MA, USA, 2013; pp. 193–198. ISBN 978-1-608-07659-8.
9. Schmidt, H.; Siedle, C. The charge equalizer-a new system to extend battery lifetime in photovoltaic systems, UPS and electric vehicles. In Proceedings of the IEEE Telecommunications Energy Conference, Paris, France, 27–30 September 1993.
10. Pognant-Gros, P.; Di Domenico, D.; Olszewski, D.; Barsacq, F. Switched Capacitor Balancing Time Estimation and Dependency. In Proceedings of the IEEE Vehicle Power and Propulsion Conference (VPPC), Coimbra, Portugal, 27–30 October 2014.
11. Kutkut, N.H. A modular non dissipative current diverter for EV battery charge equalization. In Proceedings of the IEEE Applied Power Electronics Conference and Exposition, Anaheim, CA, USA, 15–19 February 1998.
12. Kim, M.Y.; Kim, C.-H.; Cho, S.-Y.; Moon, G.-W. A cell selective charge equalizer using multi-output converter with auxiliary transformer. In Proceedings of the IEEE Power Electronics and ECCE Asia (ICPE & ECCE), Jeju, Korea, 29 May–2 June 2011.
13. Einhorn, M.; Roessler, W.; Fleig, J. Improved Performance of Serially Connected Li-Ion Batteries With Active Cell Balancing in Electric Vehicles. *IEEE Trans. Veh. Technol.* **2011**, *60*, 2448–2457. [CrossRef]
14. Lim, C.-H.; Lee, K.-J.; Ku, N.-J.; Hyun, D.-S.; Kim, R.-Y. A modularized equalization method based on a magnetizing energy for a series-connected lithium-ion battery string. *IEEE Trans. Power Electron.* **2014**, *29*, 1791–1799. [CrossRef]
15. Gallardo, J.; Romero, E.; Milanes, M.; Guerrero, M. Battery equalization active methods. *J. Power Sources* **2014**, *246*, 934–949. [CrossRef]
16. Lim, C.-S.; Kim, R.-Y.; Hyun, D.-S. Battery voltage sensorless charge equalizer using the multi-winding transformer. In Proceedings of the IEEE Vehicle Power and Propulsion Conference, Seoul, Korea, 9–12 October 2012.
17. Park, D.-J.; Choi, S.-Y.; Kim, R.-Y.; Kim, D.-S. A novel battery cell balancing circuit using an auxiliary circuit for fast equalization. In Proceedings of the IEEE IECON, Dallas, TX, USA, 29 October–1 November 2014.
18. Park, Y.-H.; Choi, S.-Y.; Choi, Y.-J.; Kim, R.-Y.; Cho, J.-T. A novel charge equalizer with auxiliary circuit to control the allowable charging and discharging current of the Lithium-ion battery. In Proceedings of the IEEE nternational Future Energy Electronics Conference and ECCE, Kaohsiung, Taiwan, 3–7 June 2017.
19. Li, S.; Mi, C.C.; Zhang, M. A High-Efficiency Active Battery-Balancing Circuit Using Multiwinding Transformer. *IEEE Trans. Ind. Appl.* **2013**, *49*, 198–207. [CrossRef]
20. Kutkut, N.H.; Wiegman, H.L.N.; Divan, D.M.; Novotny, D.W. Design considerations for charge equalization of an electric vehicle battery system. *IEEE Trans. Ind. Appl.* **1999**, *35*, 28–35. [CrossRef]
21. Park, H.-S.; Kim, C.-E.; Moon, G.-W.; Lee, J.-H.; Oh, J.K. Two-Stage Cell Balancing Scheme for Hybrid Electric Vehicle Lithium-Ion Battery Strings. In Proceedings of the IEEE Power Electronics Specialists Conference, Orlando, FL, USA, 17–21 June 2007.
22. Bonfiglio, C.; Roessler, W. A cost optimized battery management system with active cell balancing for lithium ion battery stacks. In Proceedings of the IEEE Vehicle Power and Propulsion Conference, Dearborn, MI, USA, 7–11 September 2009.
23. Hsieh, Y.-H.; Liang, T.-J.; Chen, S.-M.O.; Horng, W.-Y.; Chung, Y.-Y. A Novel High-Efficiency Compact-Size Low-Cost Balancing Method for Series-Connected Battery Applications. *IEEE Trans. Power Electron.* **2013**, *28*, 5927–5939. [CrossRef]
24. Uno, M.; Kukita, A. Single-Switch Single-Transformer Cell Voltage Equalizer Based on Forward–Flyback Resonant Inverter and Voltage Multiplier for Series-Connected Energy Storage Cells. *IEEE Trans. Veh. Technol.* **2014**, *63*, 4232–4247. [CrossRef]
25. Hasan, M.K.; Habib, A.A.; Islam, S.; Ghani, A.T.A.; Hossain, E. Resonant Energy Carrier Base Active Charge-Balancing Algorithm. *Electronics* **2020**, *9*, 2166. [CrossRef]
26. Wang, S.-C.; Liu, C.-Y.; Liu, Y.-H. A Non-Dissipative Equalizer with Fast Energy Transfer Based on Adaptive Balancing Current Control. *Electronics* **2020**, *9*, 1990. [CrossRef]
27. Lee, Y.-L.; Lin, C.-H.; Yang, S.-J. Power Loss Analysis and a Control Strategy of an Active Cell Balancing System Based on a Bidirectional Flyback Converter. *Appl. Sci.* **2020**, *10*, 4380. [CrossRef]
28. Choi, Y.-J.; Cha, H.-R.; Jung, S.-M.; Kim, R.-Y. An Integrated Current-Voltage Compensator Design Method for Stable Constant Voltage and Current Source Operation of LLC Resonant Converters. *Energies* **2018**, *11*, 1325. [CrossRef]